Eddy-Memory mode of multi-decadal variability in residual-mean ocean circulations with application to the Beaufort Gyre

GEORGY E MANUCHARYAN* AND ANDREW F THOMPSON

Division of Geological and Planetary Sciences, California Institute of Technology, Pasadena, CA 91125, USA

MICHAEL A SPALL

Department of Physical Oceanography, Woods Hole Oceanographic Institution, Woods Hole, Massachusetts, MA, 02540, USA

ABSTRACT

The mesoscale eddy field shapes the response of the Beaufort Gyre to temporal and spatial fluctuations in Ekman pumping, such that the eddy diffusivity controls the time scale of the gyre equilibration. Traditional eddy parameterizations suggest that this adjustment is exponential in time. Here, we use an idealized eddy-resolving gyre model and a theoretical analysis to identify the existence of a multi-decadal mode of the gyre variability related to eddy persistence. The mode manifests during the gyre spin-up causing the gyre's freshwater content to overshoot its equilibrium value by 2000 km^3, or 15% of the mean. We demonstrate that this overshoot can be predicted by diagnosing a time scale associated with mesoscale eddy memory, $\gamma \approx 6$ years, which impacts eddy buoyancy transport.

We propose an improvement to the Gent-McWilliams eddy parameterization that accounts for this eddy memory. Eddy memory gives rise to an oscillatory, but damped, mode of decadal variability. This mode has a period $T = 2\pi\sqrt{T_e\gamma} \approx 50$ years, where $T_e \approx 10$ years is the eddy diffusion time scale. The eddy-memory mode increases the Ekman-induced freshwater content variance by $\gamma/T_e = (50 \pm 15)\%$; the increase in variance is greatest for decadal trends in Ekman pumping. The identification of variability associated with eddy memory highlights the need for better observational constraints of Arctic eddy characteristics. We expect that eddy memory is a general property of current systems where eddies play a leading order role in balancing the mean forcing, and thus the the results are broadly applicable to many oceanic regions.

1. Introduction

The Beaufort Gyre, a major anticyclonic circulation feature in the Arctic Ocean, hosts a substantial fraction of the overall Arctic freshening (*Haine et al* 2015). The large-scale gyre circulation has been directly linked to its freshwater content (FWC) via the process of Ekman pumping that converges relatively fresh surface waters and deepens the halocline (e.g. *Proshutinsky et al* 2002). The Ekman pumping arises due to transient anticyclonic winds that cause significant gyre variability on interannual and longer time scales. However, observations indicate that the halocline depth (roughly equivalent to the FWC) varies, but does not always mimic, the variability in the strength of the anticyclonic wind stress (e.g *Proshutinsky et al* 2009; *Giles et al* 2012). Understanding and modeling the variability of the large-scale gyre circulation and the associated FWC remain a challenging problem.

The availability of FW sources, the strength of Ekman pumping, and interactions with the Atlantic layer are all factors external to the large-scale circulation that have been studied with respect to Beaufort Gyre variability(*Proshutinsky et al* 2002; *Giles et al* 2012; *Martin et al* 2014; *Morison et al* 2012; *Stewart and Haine* 2013; *Lique and Johnson* 2015; *Lique et al* 2015). A recent study, however, emphasized the internal dynamics of the gyre and demonstrated that the large-scale halocline deepening due to Ekman pumping is counteracted by the cumulative action of mesoscale eddies (*Manucharyan and Spall* 2016) – a dynamical balance similar to that of the Antarctic Circumpolar Current (ACC) (*Marshall and Radko* 2003) or the Weddell Gyre (*Su et al* 2014). Unlike the ACC, which is in the eddy-saturated regime with weak variability of its transport (*Tansley and Marshall* 2001; *Hallberg and Gnanadesikan* 2001; *Munday et al* 2013), the Beaufort Gyre appears to be highly sensitive to variations in the Ekman pumping (*Proshutinsky et al* 2002; *Manucharyan and Spall* 2016). This implies that a continuing melting of the the sea ice and/or changes in the atmospheric winds that alter the Ekman pumping would lead to substantial

---

Corresponding author address: Georgy E Manucharyan, MC 131-24, California Institute of Technology, 1200 East California Boulevard, Pasadena, CA, 91125, USA.
E-mail: gmanuch@caltech.edu

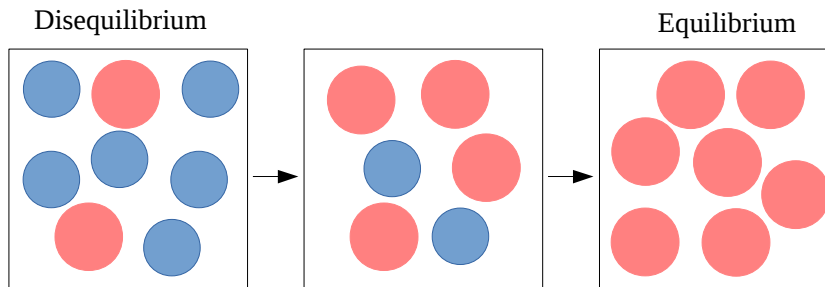Disequilibrium   Equilibrium

FIG. 1. Conceptual representation of the mesoscale eddy field illustrating the persistence of eddies in time during the equilibration process (e.g. during an Ekman-driven spin up). Red eddies have statistical properties that correspond to the equilibrium state, while blue eddies correspond to an earlier equilibrium state. The transitional eddy field (middle panel) is a mixture of the different type of eddies.

changes in the halocline depth and hence in the freshwater budget of the entire Arctic Ocean.

Manucharyan et al (2016) point out that the eddy field plays a key role in gyre variability by providing buoyancy fluxes comparable to Ekman-driven buoyancy transport. In addition, they demonstrate that, due to eddies, a large-scale circulation viewed in an ensemble mean sense (i.e. averaged over small scale eddies and waves) is a stable dynamical system that equilibrates on a time scale controlled by eddy diffusivity. However, their conclusion relies upon the use of a conventional Gent-McWilliams (GM) eddy parameterization (*Gent and McWilliams* 1990) that takes the eddy thickness fluxes to be proportional to the large-scale halocline thickness gradients

$$\overline{\mathbf{v}'h'}(\mathbf{x},t) = -K\overline{\nabla h}(\mathbf{x},t), \qquad (1)$$

where $\mathbf{v}'$ and h' are the velocity and halocline thickness perturbations due to time-dependent motions and the overbar denotes an ensemble average. A key assumption of the GM parameterization, which is to be challenged in this manuscript, is that the eddy fluxes at a particular point in time and space depend only on the large-scale state of the ocean at the same point in time and space.

The assumption of temporal and spatial locality can be questioned from both observational and numerical modeling evidence. Observations suggests that mesoscale eddies (in a form of coherent vortices) can persist in the open ocean for years, propagating large distances from their formation regions (*Chelton et al* 2011). With respect to the Arctic Ocean, using a numerical model *Spall et al.* (2008) discuss how shelf-break eddies propagate away from their formation region, and can be further transported by the mean current of the Beaufort Gyre. *Manucharyan and Timmermans* (2013) discuss a self-propagation mechanism of sub-mixed layer Arctic eddies that are observed to advect the buoyancy and potential vorticity anomalies up to 500 km away from their presumed formation regions

(*Timmermans et al.* 2008). Thus, it is reasonable to assume that a large-scale eddy field does not only depend on a current state of the ocean but carries a finite memory of its past states and a history of dissipative processes.

We illustrate the persistence of eddy properties schematically in Fig. 1. Consider the equilibration of an ocean that is populated with 'blue' eddies that are less energetic than the equilibrium-type 'red' eddies (Fig. 1, left panel). By different types of eddies we imply the existence of statistical eddy properties, *i.e.* sizes, eddy kinetic energy or eddy transport, that are generated by the mean flow. While the mean currents are generating the red-type eddies, the number of blue-type eddies will be decreasing as they are dissipated or absorbed by the mean flow (Fig. 1, middle panel). Eventually, the ocean will be populated only with the equilibrium-type 'red' eddies (Fig. 1, right panel). Since the eddy transport is associated with an eddy field that has a memory, it is important to understand how it feeds back on the evolution of the large-scale current.

In this manuscript, we use an idealized model of the Beaufort Gyre (Section 2) to present evidence that eddy-memory significantly affects the dynamics of the eddying current (Section 3). We discuss dynamical constraints that a conventional local in time GM-parameterization imposes on large-scale ocean dynamics (Section 4) and suggest an improvement that includes the eddy-memory effect (Section 5). Using the new eddy parameterization we discover a low-frequency internal mode of variability of the large-scale flow (Section 6). Characteristics of the mode and its effects on the variability of the ocean circulation are assessed in Section 7. We summarize in Section 8.

2. Model configuration

We use an idealized model of the Beaufort Gyre in a configuration identical to the one used in *Manucharyan and Spall* (2016) (see appendix A therein). The gyre is represented by a cylindrical ocean basin (diameter 1200
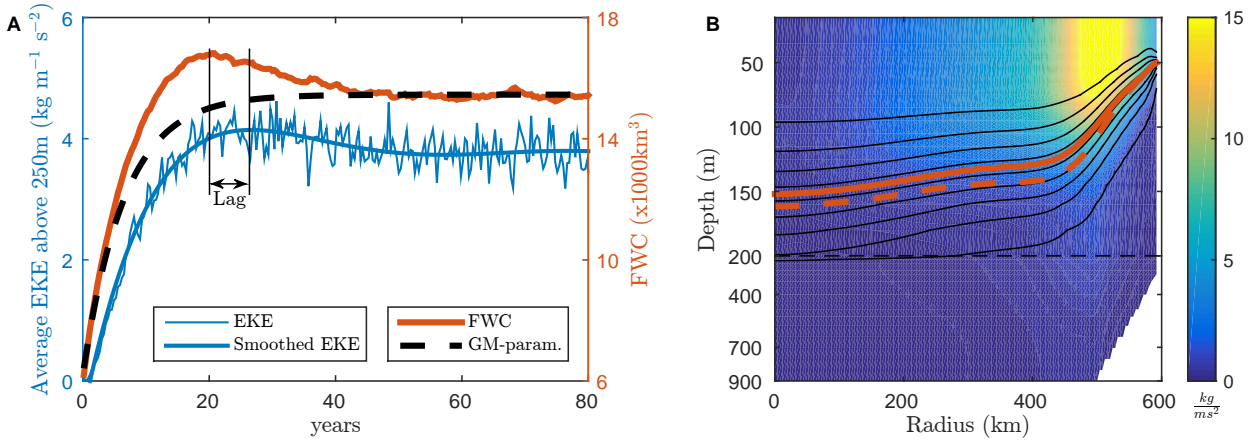
FIG. 2. **A.** Equilibration of the simulated Beaufort Gyre from rest (initial halocline depth is spatially-uniform at 50 m) for the reference case $\hat{\tau} = 0.015$ N m^{-2}. The time evolution of the freshwater content (FWC, red curve) and the theoretical prediction based on the GM parameterization (black dashed curve) is given by the right-hand y-axis. The FWC overshoots its equilibrium value by about 2000 km^3. The evolution of the domain-integrated EKE $= = \rho(u^2 + v^2)/2$ (thin blue curve, units kg m^{-1} s^{-2}) and a 5th order polynomial fit to the EKE time series (thick blue curve) is shown by the left-hand y-axis. The EKE maximum lags the FWC maximum by about 7 years. **B.** Equilibrium distribution of EKE (color, kg m^{-1} s^{-2}); the maximum EKE is over the continental slope where baroclinicity is strong. Contours indicate the equilibrium salinity distribution (isohalines between 29 and 34 spaced by 0.5). The equilibrium halocline, $S = 31.25$, and the halocline location at $t = 20$ years (time of maximum overshoot) are given the solid and dashed red curves, respectively. The vertical axis has been squeezed by a factor of 8 in a region below 200 m where the stratification and EKE are weak.

km, depth 900 m) driven by an anticyclonic surface-stress $\tau(r)$ corresponding to a uniform Ekman pumping. The fluid dynamical equations are solved using the MIT General Circulation Model in its three-dimensional hydrostatic configuration. A 4 km horizontal resolution along with variable in depth vertical resolution between 10m to 60m is sufficient to permit Rossby deformation scale eddies (the baroclinic deformation radius is about 20 km in these simulations). The salinity profile is restored at the edges of the gyre to a fixed salinity profile that consists of a 50 m deep surface layer of relatively fresh waters of salinity 29, followed by a lower layer of salinity 34 (values are chosen to mimic the hydrography of the Beaufort Gyre (*Steele et al* 2001)). Restoring leads to a fixed halocline depth at the gyre boundaries. This configuration, as highlighted in earlier studies (*Manucharyan and Spall* 2016; *Manucharyan et al* 2016), provides an infinite reservoir of freshwater and thus the results here should be treated as an upper bound on the possible fluctuations in the halocline volume . Consistent with *Manucharyan and Spall* (2016), we include a continental slope: lateral boundaries are vertical down to 300 m, below which the depth increases linearly to the bottom of the basin penetrating 100 km towards the center of the gyre (see Fig. 2b). Note that *Manucharyan et al* (2016) considered a flat topography case, which is more applicable to the interior of the gyre. However, we demonstrate in Section 8 that the continental slope is essential for the gyre dynamics discussed here.

3. Signatures of eddy memory

Spin up simulations are initialized with a horizontally uniform stratification (50 m initial halocline depth) and forced with a spatially uniform, temporally-invariant, Ekman pumping (corresponding to a linear surface stress profile $\tau_0 = \hat{\tau} r/R$). Following the development of the mesoscale eddy field, the idealized Beaufort Gyre model achieves a statistically-steady state after several decades (Fig. 2a). Note that this time scale is significantly longer than the 5 year long e-folding equilibration in a flat-basin case considered in *Manucharyan et al* (2016). The prolonged equilibration is entirely due to the presence of a continental slope in our simulations. The slope suppresses the development of instabilities and locally reduces the mesoscale eddy diffusivity (*Isachsen* 2011; *Stewart and Thompson* 2013) that leads to an enhanced eddy diffusion time scale. Note that, because the gyre dynamics are governed by a halocline thickness diffusion equation, any localized reduction in the eddy diffusivity would have a strong influence on the equilibration time scale as well as on the halocline depth.

The equilibrium corresponds to a vanishing residual circulation that is supported by the mesoscale eddy buoyancy transport that counteract the Ekman transport. Most of the eddy kinetic energy is concentrated in the upper layer corresponding to the first baroclinic mode (see Fig. 2b). Characteristic eddy velocities in the upper 200 m of the

gyre are 0.05–0.1 m s^{-1}. These eddies are about 100–200 km in diameter but are relatively weak compared to more intense but smaller scale sub-mixed layer eddies (about 20km in diameter) commonly observed via the Ice Tethered Profilers (*Zhao et al* 2014). Suggesting a significant inverse cascade of energy, these larger scale eddies are nonetheless responsible for maintaining key properties of the halocline such as its depth and adjustment time scale.

In these simulations, the FWC, conventionally defined as a domain integrated measure of salt content relative to a reference salinity S_{ref}, is directly proportional to the volume of water above the halocline V and to the salinity difference ΔS across the halocline:

$$FWC = \frac{\Delta S}{S_{ref}}V, \text{ where } V = 2\pi \int_0^R hr dr \qquad (2)$$

and h is the halocline depth. While the equilibration of the gyre FWC and eddy kinetic energy (EKE) can be crudely viewed as an exponential adjustment, a closer consideration reveals important deviations (Fig. 2a). In particular, there exists a significant overshoot of the FWC that lasts for several decades (Fig. 2a, red curve). The maximum depth of the halocline (at year 30) is up to 10–15 m deeper than its equilibrium value (Fig. 2b). This corresponds to an FWC overshoot of about 2000 km^3 (Fig. 2a), which is comparable to an observed Beaufort Gyre FWC increase of 3000km^3 over the past two decades (*Haine et al* 2015). The halocline deepens beyond its equilibrium because the eddy field is insufficiently energetic to counteract the Ekman transport for a transient period due to the weaker eddies generated during the early stages of the spin up. After the halocline reaches its deepest levels the eddy field becomes overly energetic generating excessive thickness fluxes that reduce the halocline depth. This cycle is manifested as an overshoot in the EKE that is lagged with respect to the FWC by about 5-7 years (Fig.2a, blue curve).

These lagged overshoots in EKE and FWC are signatures of an oscillatory mode that operates in addition to the exponential decay. Since we observe only one full oscillation before the gyre equilibrates, this mode is heavily damped and needs external forcing to be sustained. Nonetheless, the existence of this damped mode can not fit into our traditional understanding of the mesoscale eddy dynamics as viewed through the lens of the local in time GM-parameterization.

4. Dynamical implications of GM parameterization

Here we briefly discuss the conventional GM parameterization and a key constraint that it imposes on the evolution of large-scale flows. In particular, we focus on the dynamics of a large class of currents that are forced by transient Ekman pumping with non-zero mean. When the diabatic forcing is small compared to the mean Ekman pumping, the time-averaged state corresponds to a vanishing residual mean circulation. Transient forcing, however, can produce significant deviations from the equilibrated state.

The GM-parameterization operates under the assumption of slowly-evolving ocean dynamics such that at any given moment in time and space the mesoscale eddy field can be considered in equilibrium with local, large-scale currents. In particular, it assumes that the eddy streamfunction $\psi^* = K(s)s$ is proportional to the time-dependent halocline slope $s(t)$ and an eddy diffusivity K that can be slope-dependent (*Visbeck et al.* 1997), but is typically not time dependent. Near its mean state the perturbation eddy streamfunction $\psi'^* = K's_0 + K(s_0)s'$ can be expressed as

$$\psi'^*(r,t) = \tilde{K}(r)s'(r,t), \qquad (3)$$

where $\tilde{K}$ is the constant in time eddy diffusivity for the perturbations

$$\tilde{K}(r) = \left[\frac{dK}{ds}s_0 + K\right]_{s=s_0}. \qquad (4)$$

and $s_0(r)$ is the equilibrium halocline slope (primes denote perturbations from equilibrium). Note, that the eddy diffusivity for a linearized system can be different from the background diffusivity *i.e.* $\tilde{K} \neq K(s_0)$. Thus, if one assumes a linear dependence of the eddy diffusivity on halocline slope (*Visbeck et al.* 1997), which is appropriate for the Beaufort Gyre (*Manucharyan et al* 2016), then $\tilde{K} = 2K(s_0)$.

The halocline thickness evolution under the GM-parameterization obeys a forced diffusion equation:

$$h_t = \frac{1}{r}\left(\tilde{K}rh_r\right)_r + w_E, \qquad (5)$$

where $w_E(r,t)$ is the time-dependent Ekman pumping. We have used cylindrical coordinates, where r is the radial coordinate. A full derivation of the halocline tendency equation for perturbation variables can be found in Appendix A of *Manucharyan et al* (2016). The eddies act as a thickness diffusion because GM parameterization assumes the eddy thickness flux to be proportional to the halocline slope ($\psi^* \sim h_r$).

Equation 5 allows to get further insight into the halocline volume dynamics. Consider the least damped eigenfunction $\bar{h}$ of the diffusion operator on the right hand side of Eq. (5)

$$\frac{1}{r}\left(r\tilde{K}\bar{h}_r\right)_r = -\frac{\bar{h}}{T_e}, \qquad (6)$$

where T_e (inverse of the smallest eigenvalue) defines the gyre equilibration time scale. *Manucharyan et al* (2016) demonstrate that higher mode eigenfunctions of this eddy diffusion operator are highly damped (damping time scale increases quadratically with the number of zero crossings)

and hence only the least damped eigenfunction can significantly contribute to changes in the halocline volume. Thus, integrating Eq. 5 over the domain, keeping only a contribution from the least-damped eigenmode, and using Eq. 6 we arrive at

$$\dot{V} = -\frac{V}{T_e} + W_E, \tag{7}$$

where the over-dot indicates the time derivative and W_E is the Ekman transport (domain integrated Ekman pumping projection onto the least damped eigenmode). Eq. 7 demonstrates that under the GM-parameterization the large scale currents are constrained to equilibrate exponentially *i.e.* no internal oscillations are possible. Numerical simulations, however, demonstrate that an eddying current can significantly deviate from exponential equilibration (Fig. 2) exhibiting oscillatory behavior that cannot be captured by the local in time GM-parameterization.

5. Eddy memory parameterization

Here we introduce an improvement to the GM parameterization by accounting for the eddy-memory and validate its relevance in the eddy resolving model.

a. Parameterization

We make a key assumption that the eddy streamfunction has a finite memory of past states

$$\psi^*(t) = \frac{1}{\gamma} \int_{-\infty}^{t} \tilde{K} s(t') \exp\left(-\frac{t-t'}{\gamma}\right) dt', \tag{8}$$

where γ is the eddy-memory time scale and this definition is applicable for sufficiently small perturbations away from the mean state such that $\tilde{K}$ does not depend on slope perturbations s. This integral form implies that the present eddy transport (at time t) consists of contributions of past transports (at times $t' < t$) with weights that are exponentially decreasing with time towards the past. Contributions from past transports quantify the eddy persistence (see Fig 1 and discussions thereof). Note, that in the limit of no memory, $\gamma \to 0$, or in equilibrium, $s(t) = const$, this parameterization (Eq. (8)) is identical to the conventional GM-parameterization (Eq. (4)).

Since $\tilde{K}$ is a defined by the mean state and hence is independent of time, our parameterization can be written in the following way

$$\psi^*(t) = \tilde{K} s^*(t) \tag{9}$$

$$s^*(t) = \frac{1}{\gamma} \int_{-\infty}^{t} s(t') \exp\left(-\frac{t-t'}{\gamma}\right) dt'. \tag{10}$$

where we have defined an effective slope s^* that contains memory of past transports and governs the eddy transport. Alternatively, one can define an effective eddy diffusivity

$K_{eff} = \tilde{K} s^*/s$ such that $\psi^* = K_{eff} s$. The effective diffusivity, however, is not a physically relevant quantity and it can be inconvenient to use in practice. For example, K_{eff} is unbounded when eddies generated in the past are still contributing to the transport while a present slope is negligibly small (i.e. $K_{eff} \to \infty$ when $s \to 0$). However, an extremely large K_{eff} is misleading since a physically relevant eddy transport ($\psi^* = K_{eff} s$) is finite. Hence, K_{eff} can not be directly interpreted as a measure of the mesoscale eddy activity. We thus choose to proceed with our analysis using the effective slope s^* (Eq. 10) as a physically relevant and singularity-free quantity that defines the eddy thickness transport.

Differentiating Eq. (10) with respect to time leads to

$$\frac{ds^*}{dt} = -\frac{s^*}{\gamma} + \frac{s}{\gamma}. \tag{11}$$

Integrating Eq. 11 forward in time is an efficient and simple method of calculating s^* in numerical models as it avoids heavy calculations of the integral in Eq. (10) at every time step. Note, that the eddy memory can lead to periods of up-gradient thickness transport when s^* and s have different signs. However, Eq. 11 implies that the eddy memory does not affect steady or slowly-evolving mean currents for which $s^* \approx s$ and hence the long term average of the eddy thickness transport is always down-gradient.

b. Diagnosing eddy memory

We now quantify the impact of the eddy memory as it relates to the eddy thickness transport in the eddy resolving Beaufort Gyre model. We diagnose time series for the eddy streamfunction $\psi^*(t)$ by calculating the eddy thickness fluxes during the gyre spin up simulation. Fig. 3a demonstrates that $\psi^*(t)$ and $s(t)$ when plotted against each other have a relationship characteristic of a spiral sink. First, the eddy field and halocline slope do not equilibrate following a conventional straight line path predicted by the GM-parameterization, e.g. the blue curve has large deviations from the straight line in Fig. 3a. Instead, away from equilibrium the eddy streamfunction evolves more slowly compared to the halocline slope (blue curve is above the dashed black curve in 3a). Second, the diagnosed ψ^* and s loop approaches the equilibrium in a spiraling trajectory with a quickly decaying radius of the spiral (see the black arrows around $0,0$ in Fig 3a).

We do not know the value of γ *a priori*, but we can attempt to infer it by assessing the correlation between the eddy streamfunction and the effective slope defined by Eq. 10. Calculations show that there is indeed an optimal value of $\gamma \approx 6$ years that enhances the correlation (Fig. 3b, blue curve). Throughout the gyre equilibration ψ^* is better approximated as a linear function of s^* rather than s (Fig.
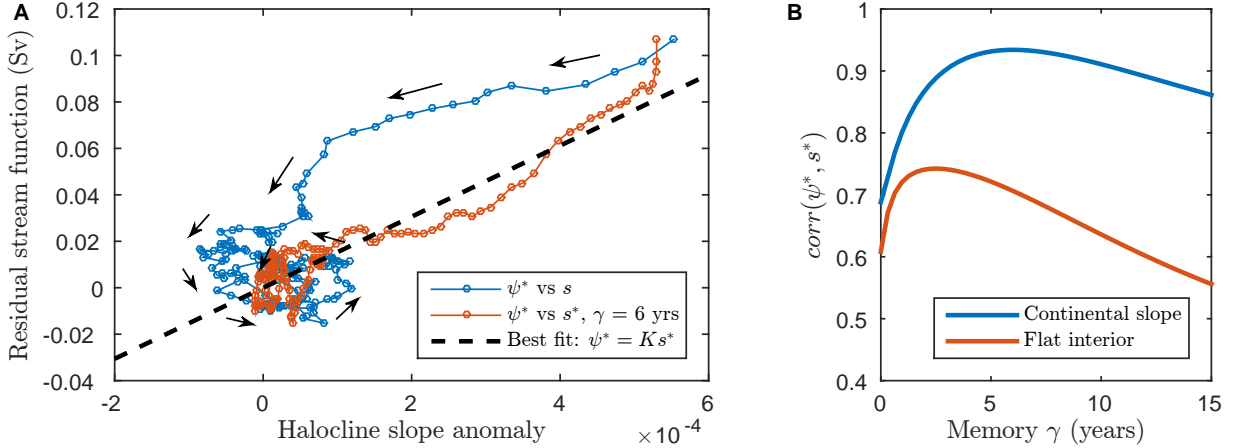
FIG. 3. **A.** Eddy streamfunction plotted as a function of the halocline slope s anomaly (blue curve) and as a function of the effective halocline slope anomaly s^* for the optimal memory (red curve). Arrows denote the direction of increasing time. A linear fit $\psi^* = Ks^*$ ($K = 150m^2s^{-1}$) is given by the dashed line. **B.** Correlation between the residual streamfunction ψ^* and the effective halocline slope s^* (Eq. 10) plotted as a function of the eddy memory γ for two regions: (i) over the sloping bottom near the boundary ($r = 550$ km) (blue curve) and (ii) in the interior of the gyre ($r = 400$ km, red curve). The optimal memory time scale is the value of γ that maximizes the correlation.

3a), with the best linear fit of $\tilde{K} = 150$ m^{2}s^{-1} (Fig. 3a, black dashed line).

The inferred eddy diffusivity $\tilde{K}$ is smaller than the value reported in *Manucharyan et al* (2016) because of the continental slope that in our model suppresses baroclinic instabilities. The continental slope also plays a major role in enhancing the eddy memory, since in the interior of the gyre $\gamma \approx 2$ years (Fig. 3b, red curve). This suggests that there might be a relation between the magnitude of eddy memory and the eddy adjustment time scale that is inversely proportional to the eddy diffusivity. Thus, for regions with high eddy diffusion the eddy memory is small and vice versa.

6. Emergence of the Eddy-Memory mode

Now that we have established the physical basis and diagnosed the eddy memory in the gyre we proceed to reveal the newly emerging dynamics. Applying our modified GM parameterization, the perturbations in halocline depth h with respect to the equilibrium or mean state of the gyre evolve following thickness diffusion equation

$$h_t = \frac{1}{r}\left(\tilde{K}rh_r^*\right)_r + w_E, \qquad (12)$$

$$h_t^* = -\frac{h^*}{\gamma} + \frac{h}{\gamma}, \qquad (13)$$

where we have introduced an effective halocline depth h^* as $h_r^* = s^*$. The two terms on the right hand side of Eq. 12 represent the divergence of the eddy thickness flux and the Ekman pumping. Note that we consider axisymmetric solutions in cylindrical coordinates and all variables in

Eqns. 12-13 are perturbations from the equilibrium state corresponding to forcing by the mean Ekman pumping.

Combining the equations above to eliminate h^* we obtain

$$h_{tt} + \frac{1}{\gamma}h_t = \frac{1}{\gamma}\left[\frac{1}{r}\left(r\tilde{K}h_r\right)_r\right] + \left(\dot{w}_E + \frac{w_E}{\gamma}\right). \qquad (14)$$

Note that the model diagnosed eddy memory is spatially inhomogeneous, but for simplicity of the analytical analysis we are assuming a constant parameter γ which should be interpreted as an effective memory that affects the bulk gyre dynamics. In the absence of forcing ($w_E = 0$) this equation describes the equilibration of the gyre by exponentially damped waves. To further illuminate the dynamics lets consider the evolution of the halocline volume V. Domain integrating Eq. 14, keeping only a contribution from the least damped eigenmode, and using Eq. 6 we arrive at

$$\underbrace{\ddot{V} + \frac{1}{\gamma}\dot{V} + \frac{1}{\gamma T_e}V}_{\text{Damped oscillator}} = \underbrace{\dot{W}_E + \frac{W_E}{\gamma}}_{\text{Ekman forcing}}, \qquad (15)$$

where the over-dot indicates the time derivative and W_E is the Ekman transport (as in Eq. 7).

Eq. 15 illuminates the core internal dynamics behind the equilibration of the halocline – an externally forced damped oscillator. The ratio of the eddy memory to the eddy adjustment time scale (γ/T_e) determines whether solutions are either over-damped (non-oscillatory) or under-damped (oscillatory). Note that in the absence of memory (a limit of $\gamma \to 0$) Eq. 15 becomes identical to an exponential decay equation 7 derived using a conventional
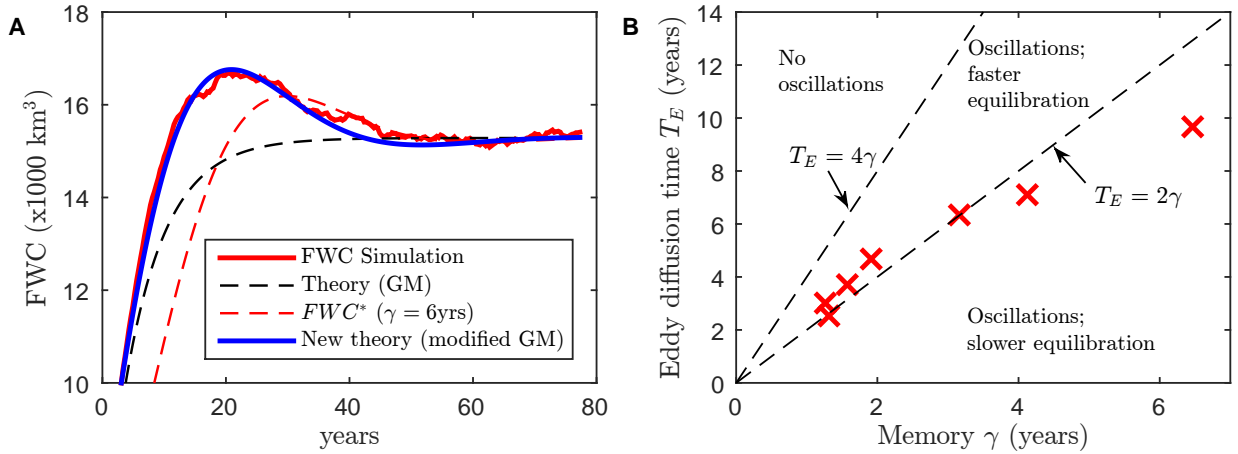
FIG. 4. **A.** FWC equilibration for the Beaufort Gyre spin-up simulation in an eddy-resolving model (red curve) and its theoretical prediction based on the GM-parameterization (black dashed line). The modified theory that includes the eddy-memory effect is shown in blue; the effective value of FWC^* is given by the dashed red curve (FWC^* is defined by Equation 2 using h^* instead of h). **B.** The relationship between eddy memory (γ) and the eddy diffusion time scale (T_e) as diagnosed from a series of numerical simulations of the Beaufort Gyre forced by different Ekman pumping. T_e diffusion time scale is smaller for large Ekman pumping because of the larger eddy diffusivities. Dashed curves show boundaries between the dynamical regimes as determined from Eq. 17: $\gamma/T_e = \{0.25, 0.5\}$.

GM-parameterization. However, if the eddy memory is sufficiently large ($\gamma > 0.25T_e$, as shown below) the system oscillates with the frequency ω_0 expressed as:

$$\omega_0 = \sqrt{\frac{1}{\gamma T_e}}, \qquad (16)$$

and hence the period $T_0 = 2\pi\sqrt{\gamma T_e}$ would be proportional to the geometric mean between the eddy memory and eddy diffusion time scales. Using our model-based estimates for the Beaufort Gyre ($\gamma \approx 6$ years, $T_e \approx 10$ years) we obtain a period of the EM-mode $T_0 \approx 50$ years. The damping time scale for the oscillations is given by $2\gamma = 12$ years (much shorter than its period) and hence the mode is highly damped requiring continuous external forcing to be sustained. While the EM-mode has a distinct multidecadal period, its amplitude has a significant response to a wide range of forcing frequencies because of its strong damping. We speculate that the transience of the atmospheric Beaufort High pressure system can efficiently energize this mode.

Solving Equation (15) for the initial conditions from the spin up simulation (shown in Fig. 2a), taking $W_E = 0$ since there are no Ekman pumping perturbations during the spin up, and using $\gamma = 6$ years (as implied by Fig. 3b, red curve) significantly improves the theoretical prediction of the numerically diagnosed evolution of FWC (see Fig. 4a). In particular, our new theory captures the amplitude

and duration of the overshoot in addition to the overall exponential equilibration. Furthermore, it captures a lag between the peaks in FWC and the eddy transport (observe that FWC^* is proportional to ψ^* in Fig. 4a). Since the inclusion of the EM-mode dramatically improves the representation of the halocline dynamics we proceed to explore several of its major implications.

7. Role of the EM-mode in halocline dynamics

a. Halocline equilibration

The equilibration of the FWC anomalies is represented by damped oscillations that can be expressed in the form of complex exponentials $V \sim \exp(-\lambda t)$ where the real part of λ corresponds to the amplitude decay rate and the imaginary part of λ corresponds to the oscillation frequency. Plugging this solution into Equation (15) we get two possible values:

$$\lambda_{1,2} = \frac{1}{2\gamma} \pm \frac{1}{2\gamma}\sqrt{1 - \frac{4\gamma}{T_e}}. \qquad (17)$$

If $\gamma > 0.25T_e$ the solution oscillates as λ has a imaginary part. These oscillations decay in amplitude with time and for arbitrary initial conditions their decay rate corresponds to the smallest of the real parts between the two characteristic equation roots (Eq. 17). The inverse of the decay rate is the time scale of the gyre equilibration T_{eq} which depends on both γ and T_e. In the absence of memory ($\gamma \to 0$) $\lambda = 1/T_e$ and hence $T_{eq} = T_e$ consistent with an exponential gyre equilibration that was discussed in *Manucharyan*
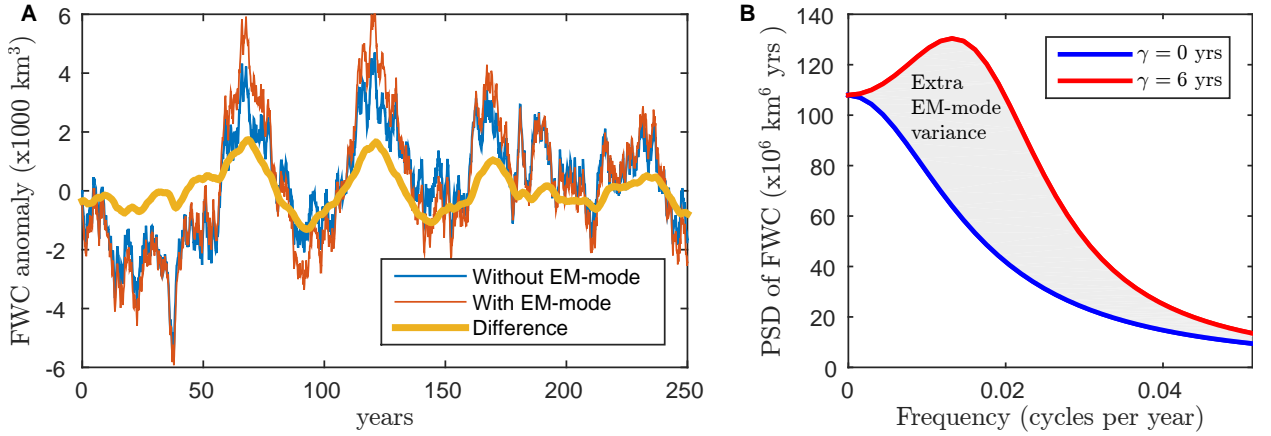
FIG. 5. **A.** Ekman-induced evolution of the FWC anomalies with eddy memory (red curve) and without eddy memory (blue curve), as simulated by Equations 15 and 7 respectively. Ekman transport (W_E) time series are represented by a white noise process with zero mean. The eddy diffusion time scale is the same for both runs ($T_e = 10$ years) and eddy memory $\gamma = 6$ years. The difference between the two time series is given by the gold curve. **B.** Power spectral density of FWC variability with eddy memory (red curve) and without it (blue curve); the spectra are indistinguishable from the theoretical predictions by Equations 18 and 19 respectively. The gray area emphasizes the enhanced variance due to the eddy memory.

et al (2016). The presence of memory $\gamma/T_e < 0.5$ leads to a reduction of the equilibration time making the gyre more stable despite the presence of the oscillations (by increased stability we imply larger decay rates). In fact, having a memory $\gamma = 0.25T_0$ reduces the equilibration time by a factor of 2. Thus, the gyre dynamics is an under-damped oscillator if $\gamma > 0.25T_0$ and is a faster-equilibrating over-damped oscillator for $\gamma < 0.25T_0$. For $\gamma > 0.5T_0$ the equilibration is slower as compared to the memoryless limit.

Our numerical simulations conducted for a wide range of Ekman pumping forcing suggest that there is a relation between the two time scales. Most of the diagnosed points lie close to $\gamma = 0.5T_e$ – a boundary at which the gyre equilibration time $T_{eq} = 2\gamma = T_e$ (as inferred from Eq. (17)) would be exactly equal to the eddy diffusion time scale. Indeed, stronger Ekman pumping forcing leads to shorter time scale because of the large eddy diffusivities. However, a strong flow would lead to a faster reduction in the persistence of the eddy field due to enhanced eddy-mean flow interactions. The opposite occurs for weak Ekman pumping. A mechanistic understanding of the parameter regime where the ratio γ/T_e is constant remains an open question.

b. Enhanced halocline variability

The FWC of the gyre in our surface-stress driven simulations is directly proportional to the halocline volume V. Consider now the variability of V for the gyre forced by transient Ekman pumping by numerically simulating Eq. 15. We take the parameters $\gamma = 6$ and $T_e = 10$ years as diagnosed from the eddy resolving model. For simplicity

we represent $W(t)$ as a white noise process that has equal energy at all frequencies and highlight the impact of the EM-mode by comparing a simulation to the case of $\gamma = 0$.

Figure 5a compares the FWC evolution with and without memory. The amplitude of FWC variations is larger with the EM-mode due to the overshoots that are particularly prominent when decadal trends are present. For example, near years 70 and 130 the EM-mode gives an additional 2000 km^3 of FWC anomaly for a gyre that would otherwise have 4000 km^3 oscillation in FWC. That is a 50% increase in the amplitude of FWC, and comparable to the observed FWC increase of 3000 km^3 in the Beaufort Gyre (*Haine et al* 2015).

It is perhaps more illustrative to assess the effects of EM-mode in a spectral space. According to Eq. 15 the spectrum of V depends in the eddy memory in the following way

$$|\tilde{V}|^2 = \sigma^2 \frac{\omega^2 + \gamma^{-2}}{(\omega^2 - \omega_0^2)^2 + \omega^2\gamma^{-2}}, \qquad (18)$$

where σ^2 represents the spectral energy of the Ekman transport W_E (a white noise process with equal energy distribution for all frequencies) and ω_0 was defined in Eq. (16). In the memoryless limit ($\gamma = 0$) we recover an expected red-noise spectrum

$$|\tilde{V}|^2 = \frac{\sigma^2}{\omega^2 + T_e^{-2}} \quad \text{when } \gamma \to 0. \qquad (19)$$

For comparison both spectra (with and without memory) are plotted in Fig 5b demonstrating an enhanced energy at

all frequencies. The two spectra approach the same values at very low frequencies (for which $s^* \approx s$) as well as at high frequencies for which Ekman pumping dominates the dynamics and eddies do not play a significant role. Note, that the frequency ω_{max} of peak EM-mode energy is significantly shifted from ω_0 towards lower values; in particular, Eq. 18 dictates that $\omega_{max} = \gamma^{-1} = \omega_0/\sqrt{2}$ when $\gamma = 0.5T_e$. However, it is the maximum relative increase of spectral energy that occurs at $\omega = \omega_0$.

We can assess a total variance of V by taking the integral of its power spectral density over all frequencies

$$Var(V) = 2 \int_0^\infty |\tilde{V}|^2 d\omega = \frac{T_e \sigma^2}{2} \left(1 + \frac{\gamma}{T_e}\right). \qquad (20)$$

Here the integral has been calculated exactly via the Cauchy's residue theorem making use of the integrand having 4 simple poles on a complex plane $z = \pm 0.5i/\gamma \pm 0.5/\gamma\sqrt{-1 + 4\omega_0^2\gamma^{-2}}$. Equation (20) implies that the EM-mode enhances the variance by a fraction $\gamma/T_e \approx (50 \pm 15)\%$. Note that the standard deviation is a square root of variance such that the contribution of the EM-mode is approximately $0.25\gamma/T_e$. Overall, the standard deviation of FWC time series is about 2000 km^3 without and 3000 km^3 with the EM-mode. Thus, Fig. 5 together with our analytical calculations demonstrate a clear enhancement of FWC variability due to the EM-mode. This extra variance is not accounted for in climate models that implement local in time eddy parameterizations.

8. Summary and discussions

An Ekman-driven eddy-resolving model of the Beaufort Gyre was used to assess the large scale impacts of the eddy memory. The key manifestations of the eddy memory are the overshoots in halocline slope and a lagged development of the eddy kinetic energy (Fig. 4). These features can not be represented by the conventional GM-parameterization that assumes time locality of eddy fluxes.

Overshoots in FWC of the simulated Beaufort Gyre reach 2000 km^3 – a magnitude comparable to FWC variations observed over the past two decades. Note, because there are no sufficient observations of the eddy field in the Arctic Ocean previous attempts to explain the gyre variability via Ekman pumping likely carry a significant uncertainty due to the eddy thickness fluxes that are unaccounted for.

Using a Transformed Eulerian Mean theory we diagnose the time-dependent eddy streamfunction ψ^* and show that it is more closely related to the effective slope s^* that takes into account the history of ocean evolution (Fig. 3a) than to the present value of isopycnal slope s (as assumed by the GM-parameterization). With Eq. 8 we have introduced an improvement of a GM-parameterization by relaxing its key assumption of time-locality. The improved

parameterization reproduces well the transient behavior of the eddy resolving gyre model (Fig. 4a).

Our theoretical analysis of the proposed parameterization reveals that the eddy-memory leads to an emergence of a decadal variability mode that has a period $2\pi\sqrt{T_e\gamma}$ (approximately 50 years for the Beaufort Gyre). Despite the EM-mode operating on multi-decadal time scales it increases the overall isopycnal slope variance by a fraction of $\gamma/T_e \approx 0.5$ that stays relatively constant for a wide range of mean forcing (Fig. 4b). This suggests that in eddy-dominated flows there might be an inverse relation between eddy-memory γ and eddy diffusivity $\tilde{K}$ (since $T_e \sim R^2/\tilde{K}$).

Note that we have identified the bulk memory of the current as it relates to the cumulative thickness transport of the eddy field. Nonetheless, specific dynamics of individual eddies that can lead to a current having a memory remains unclear. We expect the extent of memory to depend on both the eddy dissipation rate and on the intensity of the inverse energy cascade – processes that can suppress the eddy transport. However, those would inevitably affect not only eddy memory but also the eddy diffusivity.

In order to emphasize the role of eddy memory, we have made several simplifications. We have used a memory as a parameter characteristic of the entire current. However, the spatial inhomogeneity of the eddy diffusivity implies that eddy memory might also be spatially variable. Indeed, Fig. 3b demonstrates that the memory is significantly enhanced over the continental slope – a region with weakened eddy diffusivity. The halocline evolution equation (12) is valid for a general case of spatially-dependent eddy memory but its analytical treatment are too convoluted to highlight the essential dynamics. Instead, we have simulated the evolution of equations (12) and (13) in case of an enhanced memory near the coast and confirmed that our key conclusions still hold (not shown). Note that the continental slope occupies only a small portion of the gyre (about 100 km wide); however, the bulk memory that has been diagnosed from FWC evolution is close to the local memory at the continental slope. This implies that the enhanced eddy memory even in a localized regions impacts the interior gyre dynamics.

Another potentially important factor that was omitted in our theory is vertical diffusion (a diabatic process). Mixing is likely to be important over continental slope at the boundary where there are sources of water masses. In the Arctic Ocean vertical diffusivity estimates are small (order of 10^{-6} m^2 s^{-1} to 10^{-5} m^2 s^{-1}) but it might still play a role in water mass transformations. In particular, the enhanced mixing near gyre boundaries can restrict the availability of freshwater sources and thus limit the temporal variations of the FWC. In our numerical model we have used a relatively high estimate of vertical mixing of 10^{-5} m^2 s^{-1} and we have confirmed that the amplitude of the eddy-memory mode enhances when the mixing is reduced.

The climate modeling community is constantly seeking to improve predictions of the mean climate. However, it is just as important, especially in the context of recent climate change, to simulate and understand low-frequency climate variability, which is largely dictated by ocean dynamics. We have demonstrated here that mesoscale eddies provide yet another mechanism of long-time scale variability for strongly baroclinic currents such as the ACC or the Beaufort Gyre. This effect may be amplified by potential feedbacks that involve atmospheric buoyancy fluxes that are in many cases coupled with the ocean dynamics. We thus argue that the implementation of eddy parameterizations that account for eddy-memory and an assessment of their implications for coupled climate dynamics is a necessary step forward in climate modeling.

References

Andrews, D. G., and M. E. McIntyre (1976) Planetary waves in horizontal and vertical shear: The generalized Eliassen-Palm relation and the mean zonal acceleration.*J. Atm. Sci.*, 33.11 (1976): 2031-2048. APA

Chelton, D. B., Schlax, M. G., and Samelson, R. M. (2011). Global observations of nonlinear mesoscale eddies. *Prog. Oceanogr.*, 91(2), 167-216.

Davis, P. E. D., C. Lique, and H. L. Johnson (2014) On the Link between Arctic Sea Ice Decline and the Freshwater Content of the Beaufort Gyre: Insights from a Simple Process Model. *J. Climate*, 27, 8170-8184.

Ding, Y., J. A. Carton, G. A. Chepurin, M. Steele, and S. Hakkinen (2016), Seasonal heat and freshwater cycles in the Arctic Ocean in CMIP5 coupled models, *J. Geophys. Res. Oceans*, 121, 20432057.

Gent, P. R., and J. C. Mcwilliams (1990), Isopycnal mixing in ocean circulation models, *Journal of Physical Oceanography*, 20(1), 150–155.

Giles, Katharine A., et al. (2012), Western Arctic Ocean freshwater storage increased by wind-driven spin-up of the Beaufort Gyre.*Nat. Geosc.* 5.3, 194-197.

Haine, T.W. et al (2015), Arctic freshwater export: Status, mechanisms, and prospects. *Global and Plan. Change*, 125, pp.13-35.

Hallberg, R., and A. Gnanadesikan, 2001: An exploration of the role of transient eddies in determining the transport of a zonally reentrant current, *J. Phys. Oceanogr.*, 31, 3312–3330.

Hogg, A. Mc C., and J. R. Blundell (2006) Interdecadal variability of the Southern Ocean, *J. Phys. Oceanogr.*, 36.8, 1626–1645.

Isachsen, P.E., 2011. Baroclinic instability and eddy tracer transport across sloping bottom topography: How well does a modified Eady model do in primitive equation simulations? *Ocean Modelling*, 39(1), pp.183-199.

Le Bars, D., J. P. Viebahn, and H. A. Dijkstra (2016), A Southern Ocean mode of multidecadal variability, *Geophys. Res. Lett.*, 43, 2102–2110.

Lique, C., and H. L. Johnson (2015), Is there any imprint of the wind variability on the Atlantic Water circulation within the Arctic Basin?, *Geophys. Res. Lett.*, 42, 98809888.

Lique, C., H. L. Johnson, and P. E. D. Davis (2015) On the Interplay between the Circulation in the Surface and the Intermediate Layers of the Arctic Ocean *J. Phys. Oceanogr.*, 45:5, 1393-1409.

Marshall, J., and T. Radko (2003), Residual-mean solutions for the Antarctic Circumpolar Current and its associated overturning circulation, *Journal of Physical Oceanography*, 33(11), 2341–2354.

Marshall, J. (2015), Equilibration of the Arctic halocline by eddies [Abstract]. In: 20th Conference on Atmospheric and Oceanic Fluid Dynamics, Minneapolis, MN. Abstact 3.2.

Manley, T., and K. Hunkins (1985), Mesoscale eddies of the Arctic Ocean, *Journal of Geophysical Research: Oceans (1978–2012)*, 90(C3), 4911–4930.

Manucharyan, G.E. and M.A. Spall (2016), Wind-driven freshwater buildup and release in the Beaufort Gyre constrained by mesoscale eddies, *Geophys. Res. Lett.*, 43, 273–282, doi:10.1002/2015GL065957.

Manucharyan G.E., M.A. Spall, and A.F. Thompson (2016), A theory of the wind-driven Beaufort Gyre variability, *J. Phys Oceanogr.*

Manucharyan, G. E., and M.-L. Timmermans (2013), Generation and separation of mesoscale eddies from surface ocean fronts, *Journal of Physical Oceanography*, 43(12), 2545–2562.

Martin, T., M. Steele, and J. Zhang (2014), Seasonality and long-term trend of Arctic Ocean surface stress in a model, *J. Geophys. Res. Oceans*, 119, 17231738

McPhee, Miles G. (2012) Intensification of Geostrophic Currents in the Canada Basin, Arctic Ocean. *J. Clim.*, 26, 31303138.

Morison, J., Kwok, R., Peralta-Ferriz, C., Alkire, M., Rigor, I., Andersen, R. and Steele, M. (2012) Changing arctic ocean freshwater pathways. *Nature*, 481(7379), pp.66-70.

Munday, D. R., H. L. Johnson, and D. P. Marshall (2013) Eddy saturation of equilibrated circumpolar currents. *J. Phys. Oceanogr.*, 43.3, 507–532.

Proshutinsky, A., R. Bourke, and F. McLaughlin (2002), The role of the Beaufort Gyre in Arctic climate variability: Seasonal to decadal climatescales, *Geophys. Res. Lett.*, 29(23), 2100,

Proshutinsky, A. , Krishfield R, Timmermans ML, Toole J, Carmack E, McLaughlin F, Williams WJ, Zimmermann S, Itoh M, Shimada

K (2009), Beaufort Gyre freshwater reservoir: State and variability from observations. *J. Geophys. Res.: Oceans*, 114(C1).

Rabe, B., Karcher M, Kauker F, Schauer U, Toole JM, Krishfield RA, Pisarev S, Kikuchi T, Su J. (2014), Arctic Ocean basin liquid freshwater storage trend 19922012, *Geophys. Res. Lett.*,41, 961968,

Spall, M. A., R. S. Pickart, P. S. Fratantoni, and A. J. Plueddemann (2008), Western Arctic shelfbreak eddies: Formation and transport, *Journal of Physical Oceanography*, *38*(8), 1644–1668.

Steele, M., R. Morley, and W. Ermold (2001), PHC: A global ocean hydrography with a high-quality Arctic Ocean, *J. Clim.*, 14, 20792087.

Stewart, A.L. and Thompson, A.F., 2013. Connecting Antarctic cross-slope exchange with Southern Ocean overturning. *J. Phys. Oceanogr.*, 43(7), pp. 1453–1471.

Stewart, K ., and T. Haine (2013), Wind-driven Arctic freshwater anomalies, *Geophys. Res. Lett.*, 40, 61966201

Su, Z., A. L. Stewart, and A. F. Thompson. (2014), An idealized model of Weddell Gyre export variability. *J. Phys. Oceanogr.*, 44 (6), pp. 1671–1688.

Tansley, C. E., and D. P. Marshall, 2001: On the dynamics of wind-driven circumpolar currents, *J. Phys. Oceanogr.*,31, 3258–3273

Timmermans, M.-L., J. Toole, A. Proshutinsky, R. Krishfield, and A. Plueddemann (2008), Eddies in the Canada basin, Arctic Ocean, observed from ice-tethered profilers, *Journal of Physical Oceanography*, *38*(1), 133–145.

Towns J., T. Cockerill, M. Dahan, I. Foster, K. Gaither, A. Grimshaw, V. Hazlewood, S. Lathrop, D. Lifka, G. D. Peterson, R. Roskies, J. R. Scott, N. Wilkins-Diehr, "XSEDE: Accelerating Scientific Discovery", *Computing in Science & Engineering*, vol.16, no. 5, pp. 62-74, Sept.-Oct. 2014, doi:10.1109/MCSE.2014.80

Visbeck, M., Marshall J, Haine T, Spall M. (1997) Specification of Eddy Transfer Coefficients in Coarse-Resolution Ocean Circulation Models, *J. Phys. Oceanogr.*, 27:3, 381-402.

Yang, J., A. Proshutinsky, and X. Lin (2016), Dynamics of an idealized Beaufort Gyre: 1. The effect of a small beta and lack of western boundaries, *J. Geophys. Res. Oceans*, 121.

Zhao, M., M.-L. Timmermans, S. Cole, R. Krishfield, A. Proshutinsky, and J. Toole, 2014. Characterizing the eddy field in the Arctic Ocean halocline. *J. Geophys. Research, 119*.